ELSEVIER

Biophysical Chemistry 58 (1996) 39–52

Biophysical Chemistry

Temperature-, electric field- and solute-induced percolation in water-in-oil microemulsions

L. Schlicht, J.-H. Spilgies, F. Runge, S. Lipgens, S. Boye, D. Schübel, G. Ilgenfritz *

Institut für Physikalische Chemie der Universität zu Köln, Luxemburger Str. 116, D-50939 Köln, Germany

Received 22 December 1994; revised 15 March 1995; accepted 28 March 1995

Abstract

We report investigations on the percolation of the aqueous phase in water-in-oil microemulsions, comparing systems stabilized by ionic AOT and non-ionic Igepal amphiphiles. First, we briefly review the opposite effect of temperature on the two systems and compare electric conductivity with viscosity data. In the second part, we show that percolation can be induced by high electric fields resulting in a shift of the percolation curve. The electric field measurements allow to investigate the dynamics of clustering of the water droplets to form a network of percolating channels. We examine the slow build-up and the fast decay of the percolating structure, monitoring simultaneously electric conductivity and electric birefringence. In the third part we discuss the effect of some solutes on the percolation curve, especially of small molecules which act as protein denaturants and of native and denatured proteins like methemoglobin, chymotrypsin and gelatin. The spectroscopic determination of the dimerization of hemin, released from denatured hemoglobin, reflects the incorporation of the hemin monomers in the surfactant monolayer. In the gelatin system time resolved electric birefringence shows that even at low concentrations it is the macromolecule which determines the structure of the aqueous domain. In the appendix, a simple estimate of the intrinsic Kerr-constant is given for microemulsion droplets deformed in an electric field.

Keywords: Microemulsion; Percolation; Electric field; Dynamics of electric birefringence; Gelatin

1. Introduction

Mixtures of water, oil, and an amphiphile can form thermodynamically stable, optical transparent one-phase solutions (L2 phase). In these microemulsion systems structuring of water and oil domains separated by a surfactant monolayer occurs at nanometer scales (for general reviews on microemulsions see Ref. [1–4]).

Microemulsions have found wide interest from the theoretical point of view of self-organization of matter and phase behavior to practical aspects as a medium for chemical reactions, e.g., enzyme reactions [5,6]. In the nanodroplets hydrophilic and hydrophobic reactants can be brought into close contact. The application of microemulsions in (bio)technology requires a thorough knowledge of the physicochemical properties like phase behavior, transport properties, and structure. This paper aims to contribute to these questions.

The phase behavior of microemulsions has been studied extensively. One of its characteristics is the

* Corresponding author.

SSDI 0301-4622(95)00084-4

existence of a one-phase channel from the water-rich to the oil-rich side with a continuous change from normal to inverse micelles [7,8]. All water-in-oil microemulsions, where water is the minority phase, exhibit the phenomenon of percolation of the aqueous phase. This transition from a state of isolated water droplets to one with a continuous internal aqueous phase involves the aggregation of nanometer-sized water droplets to form a network of water channels.

We will compare the behavior of microemulsions stabilized by ionic and non-ionic surfactants, using Aerosol OT (diethylhexylsulfosuccinate, AOT) and Igepal CO-520 (nonylphenylpentaethyleneglycolether, IG). Many properties of the percolation process induced by temperature, electric field and solutes have been determined in the past. In the present paper we discuss specific aspects:

In the first part we compare temperature induced percolation, monitored by static electric conductivity and viscosity and point out the significant viscosity changes in the nonionic system. The second part contains experimental results on electric field induced percolation. In the chapter on solute induced percolation we examine the effect of small molecules acting as protein denaturants and of some proteins. We are interested in the different interaction of native and denatured proteins with the surfactant layer. Methemoglobin denatures in the ionic microemulsions and releases its prostethic hemin groups which form dimers in aqueous solution. We show with spectroscopic measurements that hemin is incorporated as a monomer in the surfactant phase, and determine the apparent dimerisation constant. This example directly shows that the change of the percolation curve is correlated with the incorporation of the solute in the membrane. Gelatin, the denatured form of collagen fibres, is another example of a denatured protein inducing percolation. This system provides further information on the structure of the water domains from time resolved electric birefringence measurements.

2. Materials and methods

The surfactants AOT (Sigma, MW = 444.6 g mol^{-1}, ρ = 1.14 g cm^{-3}) and IG (Aldrich, mean MW = 440.6 g mol^{-1} corresponding to an average number of five ethoxy groups, ρ = 1.00 g cm^{-3}) were used as received. DIM (di-2-ethylhexylmalate) was synthesized from malic acid and 2-ethylhexanol [9]. Methemoglobin was obtained by oxidizing oxyhemoglobin isolated from human erythrocytes with $K_3[Fe(CN)_6]$ and purifying with a Sephadex G-25 column. Potassium chloride and oils were obtained from Merck in p.a. grade, except for decahydronaphthaline (decaline) which was used as a cis/trans-mixture (> 98% pure). Chymotrypsin was purchased from Fluka and used as received. Deuterohemin was prepared from protohemin (Fluka) as described in [10]. The optical absorption spectra were obtained with a Perkin-Elmer Lambda 19 spectrometer.

Microemulsions were prepared by weighing in calculated amounts of oil, surfactant and 10 mM KCl brine (IG systems) or water (AOT systems), those containing biopolymers by titration of mixtures of surfactant and oil with the aqueous solution of the solute. Microemulsion systems are characterized by the molar water to surfactant ratio, $W_0 = n(H_2O)/n(\text{surf})$, and the molar concentration of surfactant in oil $c(\text{surf})_{oil}$.

Gelatin (Sigma, acid processed from pig skin, bloom 300, MW $\approx (9 \pm 1) \cdot 10^4$ g/mol, polydisperse) containing microemulsions were prepared by dissolving the calculated mass of gelatin in the required volume of water, heating to 55°C (that is, above the helix-coil transition temperature of the poly-L-proline-analogous type-II-trans helix of about 35°C for the given gelatin), and adding the oil at the same temperature. The systems were allowed to cool to ambient temperature under vigorous stirring. All measurements were carried out well below the transition temperature. As long as sol-state microemulsions are examined, quenching of the systems yields the same results. For characterization of the gelatin content the value $\Gamma_w = m(\text{gelatin})/100$ ml H_2O [wt.-%] is introduced which represents the concentration of gelatin with respect to the aqueous phase. Aqueous solutions are characterized by $\Gamma = m(\text{gelatin})/V_{total}$. For the given microemulsion system the value of Γ_w is about ten times higher than Γ.

Static electric conductivity was measured in a thermostated water bath ($\pm$ 0.05°C), using a WTW-LTA electrode and a Wayne-Kerr Autobalance Pre-

cision Bridge B331 ($\omega = 10^4$ rad/s). Viscosity data were obtained with a gas-tight Ubbelohde-type capillary viscometer.

For the measurement of field effects we used the apparatus described in [11]. It allows rectangular field pulses of up to 10 ms duration and 20 kV voltage. The fastest measurable relaxation times are 50 and 1 μs for the field-on and field-off side, respectively. Measurements were carried out in a cell of cylindrical geometry with Pt-electrodes (distance 1.71 cm) and a free light path of 6 mm.

The dynamics of the electric conductivity of the sample solution was measured with a current viewing resistor in series with the measuring cell. In contrast to Kerr-effect measurements no current signal can be observed after the end of the field pulse. The Kerr-effect was measured using a He–Ne laser (Uniphase, 10 mW), two polarizers (Halle), a quarter-wave-plate (Spindler & Hoyer), and an RCA IP28 photomultiplier in the standard optical arrangement: polarizer 45°, slow axis of the quarter wave plate 135° with respect to the field direction, analyzer offset angle γ from the crossed position. Angles of γ from $+5$ to $+15°$ for systems with negative and γ from -5 to $-15°$ for those with positive birefringence were used. Birefringence of the cell windows, glass plates of 2 mm thickness, was very small and could be neglected.

Transient curves of field pulse, electric current, 90° light scattering, and birefringence were collected as voltage signals with a digital storage oscilloscope (Yokogawa, 4 channels, 8 bit resolution, 100 MHz). The birefringence phase shift, $\varphi = 2\pi l \Delta n/\lambda$, was calculated from the change in relative light intensity $\Delta I/I = [\cos(2\gamma) - \cos(\varphi - 2\gamma)]/[1 - \cos(2\gamma)]$.

3. Results and discussion

3.1. Temperature-induced percolation

The formation of a microemulsion is an entropy driven process. The enthalpic term is very small since only little work is required to form the water/oil interface due to the very small interfacial tension developing between the phases separated by the surfactant monolayer [12,13].

The microscopic structure of the water and oil domains is strongly dependent on temperature. By Eicke et al. it was first observed [14] that the electric conductivity increases drastically within a range of a few degrees centigrade. Examples of temperature-induced percolation are shown in Fig. 1. We interpret this as a transition from an oil-continuous structure to one that is also water-continuous. In the IG system the maximum value observed is one to two orders of magnitude below the limiting value, $\kappa_{max} = \kappa_0 \cdot \varphi$, determined by the volume fraction φ and the conductivity κ_0 of the aqueous phase. It is still below a value which we think is more reasonable to compare: the 'Bruggeman value', $\kappa_{Br} = \kappa_0 \cdot \varphi^{1.5}$, characterizes the conductivity of a system of one non-conducting sphere in the conducting medium. This value is also reached for an ensemble of small overlapping spheres of constant volume fraction with increasing radius [15]. The fact that this value is not reached either, shows that there must be many bottlenecks and dead ends in the structure of the water phase.

It has been pointed out by Mitchell and Ninham and Israelachvili et al. [16] that the state of the system is determined by the effective 'wedge'-form of the surfactant molecule determining the packing constraints of the monolayer. This situation is depicted in Fig. 2 following closely the presentation of de Gennes and Taupin [13]. With non-ionic amphiphiles, the wedge form results from the stronger hydration of the polar groups at lower temperatures, also leading to an increased solubility of the amphiphile in water. The larger effective volume of the headgroups forces the monolayer towards a positive curvature, resulting in a water-continuous phase (large oil droplets). At higher temperatures the hydrogen bonds are broken and the polar groups are less hydrated. As a consequence, the curvature of the surfactant layer becomes negative and an oil-continuous structure is formed (isolated water droplets).

Fig. 1 shows that ionic AOT and non-ionic IG systems exhibit opposite temperature behavior. This originates from the inverse temperature dependence of the solubility of the surfactants in water. Binary water/non-ionic surfactant systems have an upper miscibility gap, while ionics do not [4]. Thus, with increasing temperature the non-ionic molecules become less soluble in water, whereas the ionic ones are even better hydrated.

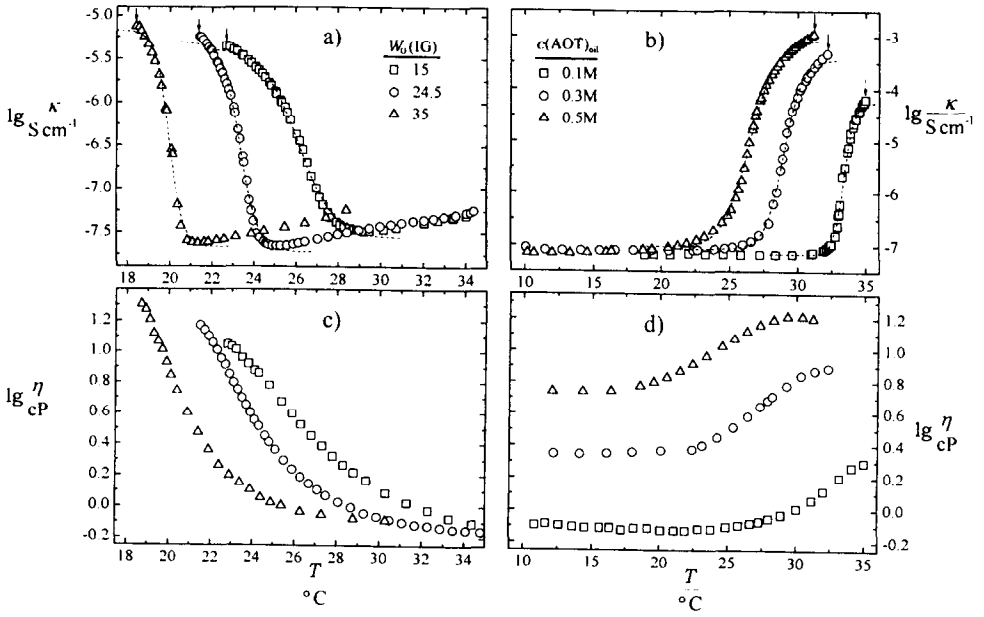

Fig. 1. Comparison of T-induced percolation as observed by measurement of electric conductivity (top) and viscosity (bottom). Left: non-ionic system (10 mM KCl/n-/c-hexane (w/w = 1:1)/IG; $c(\mathrm{IG})_{\mathrm{oil}}$ = 0.186 M) for different droplet sizes (W_0 values). Right: ionic system (water/n-heptane/AOT; W_0 = 55.5) for different droplet concentrations (amphiphile concentrations in oil). Arrows mark the phase boundaries in the percolation regime, dotted lines represent least-square-fits according to an AB-transition (see text). Van 't Hoff reaction enthalpies are in the order of 100 kJ/mol. The Bruggeman conductivity $\log(\kappa_{\mathrm{Br}}/S\ \mathrm{cm}^{-1})$ is calculated as −2.9 ($c(\mathrm{AOT})_{\mathrm{oil}}$ = 0.1 M), −2.4 (0.3 M), and −2.1 (0.5 M), respectively, for the AOT systems, and −4.8 (W_0 = 15), −4.6 (W_0 = 24.5), and −4.4 (W_0 = 35), respectively, for the IG systems.

For the AOT system it has been shown by neutron scattering that the W_0 value determines the radius R of the spherical water droplet [17]. A linear relation is found, $R/\mathrm{nm} = 0.175 \cdot W_0$, which is expected when the surfactant occupies a constant area in the interfacial monolayer.

The position of the percolation point within the one phase region for droplets of a given radius (constant W_0) depends on the concentration of the droplets. It is a characteristic result that with higher droplet concentration the percolation point moves away from the phase separation temperature, i.e., the

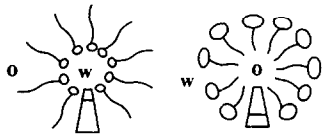

Fig. 2. Schematic model of interfacial curvature in microemulsions following [13]. W: water phase, O: oil phase. Left: w/o-microemulsion droplet, inverse micelle with negative curvature. Right: o/w-microemulsion droplet, swollen micelle with positive curvature. The curvature of a droplet is determined by the effective wedge shape of the amphiphile which is dependent on the amount of its hydration.

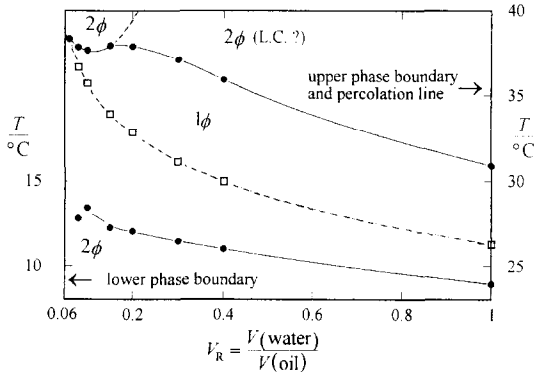

Fig. 3. Experimentally determined phase boundaries (filled circles) and percolation line (open squares) for AOT microemulsions at W_0 = 55.5 and different water to oil ratios $V_R = V_{H2O}/V_{oil}$. The volume fraction of water and surfactant for this systems is given by $\phi_{(H_2O,AOT)} = 1.39/(1.39 + V_R^{-1})$.

upper boundary in the AOT and the lower one in the IG system. This is demonstrated for AOT in Fig. 3.

There has been extensive discussion [18,19] that the conductivity percolation curves should obey universal scaling laws of percolation theory (for more details see, e.g., [20]),

$$\kappa \sim |T - T_p|^{-s}$$

with $s = 1.2$ for the low- and

$$\kappa \sim |T - T_p|^{+\mu}$$

for the high conductivity branch, where T_p defines the percolation point.

With the use of supercomputers allowing simulations with larger lattice dimensions, the theoretical value of μ has increased over the years from about 1.6 on [21–23]. Fitting results depend very sensitively on the value of T_p, where the conductivity of the lower branch diverges. We find that many AOT percolation curves can be fitted with the scaling laws using $\mu = +1.9$ [22] as well as with the present value of $\mu = +2.02$ [23].

However, in the IG system we need smaller values of s (and also of μ) for an adequate description. This especially holds for smaller droplet concentrations and larger W_0 values. In the AOT system deviations occur for $V_r < 0.2$ (cf. Fig. 3) when the percolation temperature approaches the phase boundary, as has also been observed by Cametti et al. [24].

Alternatively, all curves can be described reasonably well with the temperature dependence of a simple chemical reaction, where a species A is transformed into B. The extent of reaction x as a function of temperature, with equilibrium constant $K = 1$ at $T = T_p$, is given by:

$$x \sim \log \kappa \sim \left[1 + \exp\left\{\frac{-\Delta H(T - T_p)}{RT_p^2}\right\}\right]^{-1}$$

where ΔH is the Van 't Hoff reaction enthalpy.

This kind of formulation is analogous to the treatment of protein denaturation as a one step process. As in the denaturation case the steep transition, yielding a very high Van 't Hoff enthalpy, implies a highly cooperative process.

Fig. 1c and Fig. 1d show measurements of viscosity along the percolation transition. Comparison with the conductivity curves (Fig. 1a and Fig. 1b) demonstrates that viscosity monitors structure changes prior to the formation of the infinite network. We currently investigate to which extent the aggregation of the water droplets in microemulsions may be described by using the Baxter model of sticky hard spheres which has been applied to the rheology of aggregating alkylated silica particles [25].

Comparison of AOT with IG systems shows significant differences in the amplitude of the viscosity change which is considerably larger in the non-ionic

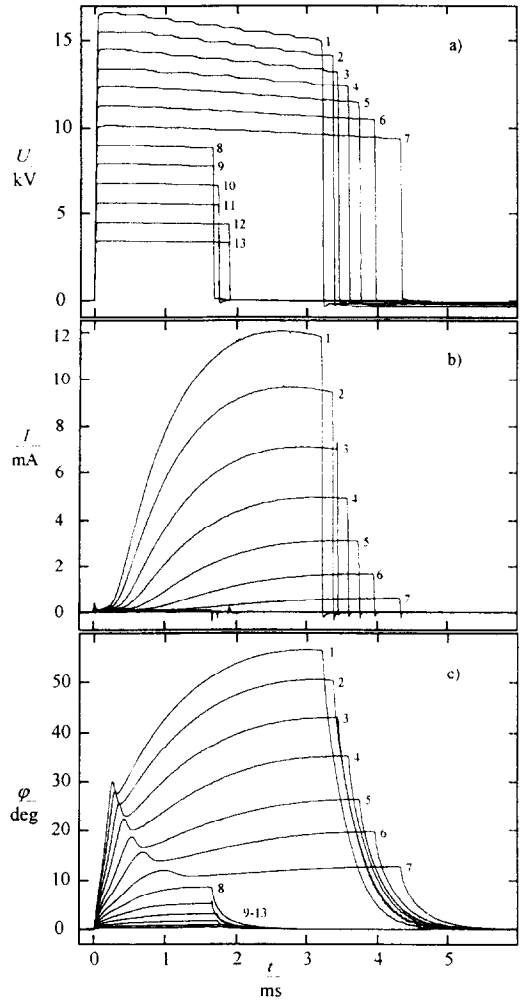

Fig. 4. Dynamics of current I and electric birefringence phase shift φ in the system water/decaline/IG ($W_0 = 24.5$, $c(IG)_{oil} = 0.186$ M) at $T = 27.4$°C ($T - T_P = +2.8$°C measured simultaneously, for different electric fields. (a) Rectangular field pulses, (b) cell current I, (c) phase shift φ.

system. The increased resistance to shear forces speaks in favor of a larger persistence length in the network structure of the percolated non-ionic system.

3.2. Electric field-induced percolation

Percolation of the aqueous phase can be induced by high electric fields as has been demonstrated for the AOT systems by Eicke et al. [26] and for the IG microemulsions by Runge et al. [11,27]. The effects of electric fields have also been studied by Tekle et al. [28].

In order to obtain information on the dynamics of the structural changes we monitor simultaneously the applied voltage pulse, the electric conductivity, the electric birefringence, and 90° light scattering as a function of time. An example of the signal curves is given in Fig. 4.

The transient conductivity data show that a threshold field strength E_c is necessary for the onset of percolation. In Fig. 4 no current flow is observed for the voltage pulses numbered from 8 onwards. E_c depends linearly on the temperature difference to the percolation point. For the IG systems the slope amounts to $dE_c/dT \approx$ 1 kV/cm K independent of droplet size (W_0 value), droplet concentration, and viscosity of the microemulsion. For AOT microemulsions this value is lower, $dE_c/dT \approx$ 0.5 kV/cm K, due to the larger polarizability of the water droplets leading to stronger interactions in the electric field. Above E_c, the conductivity curves are characterized by an induction period t_{in} before the percolation process develops in the millisecond time range. t_{in} scales exponentially with the square of the field strength: $E^2 \sim \exp\{-kt_{in}\}$.

The birefringence curves reveal that during the induction period processes take place prior to the aggregation to percolating clusters. Such fast processes comprise deformation of polarized water droplets, aggregation of droplets to small clusters, and possible orientation processes. No corresponding signal is seen during the induction period in the light scattering signal excluding the formation of larger clusters [27].

The birefringence dynamics is characteristic of a highly cooperative process: there is a slow build-up of the percolating structure in the field, where many droplets have to aggregate, but a fast decay when the field is switched off, allowing an independent disintegration at any position of the cluster. The AOT system behaves in an analogous way. Representative curves are shown in [27]. The decay dynamics is non-exponential and can be analyzed by stretched exponentials, i.e., $\varphi \sim \exp\{-(t/\tau)^{\beta}\}$ with $\beta < 1$. It

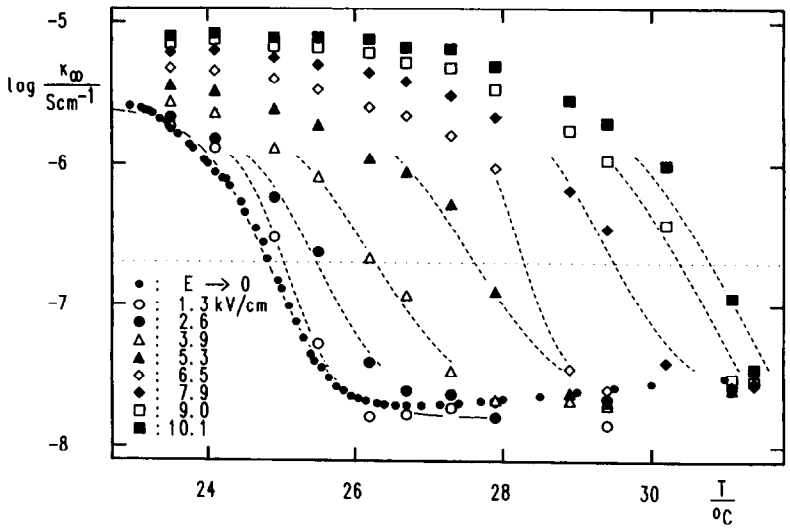

Fig. 5. Electric field induced percolation in the system water/c-hexane n-hexane w/w = 1:1 /IG (W_0 = 24.5, $c(IG)_{oil}$ = 0.186 M). The temperature induced percolation curve is shifted to higher temperatures in the electric field. κ_∞ is the final specific conductivity of the microemulsion after a stationary state has been reached in the high electric field.

is certainly controlled by diffusional processes since the time constants scale with viscosity.

There is at present no theory describing the dynamics of these aggregation processes. However, we emphasize the close analogy to the kinetics of gelation as can be described by the Smoluchowski-equation of irreversible aggregation. When $K(i,j)$ denotes the aggregation rate constant of clusters with i and j droplets, which obey the homogeneity relation $K(a \cdot i, a \cdot j) = a^{\lambda} \cdot K(i,j)$, a gelling regime is obtained for $\lambda \geq 1$ [29]. Thus, at $\lambda = 1$ the rate constants of larger clusters critically exceed those of smaller ones.

So far no explanation has been found for the overshoot phenomenon in the Kerr-signal that appears at the very moment current begins to flow. The overshoot is most pronounced at small droplet concentrations, it disappears at larger droplet concentrations where the fast and slow Kerr-processes cannot be separated anymore.

Fig. 5 demonstrates that the temperature-induced percolation curves are shifted in the electric field. The shift occurs to higher temperatures in the non-ionic and to lower temperatures in the ionic system. In contrast to the linear dependence of the critical electric field strength on temperature, there is a quadratic dependence of the percolation temperature on the field strength. The high-field conductivity exceeds the maximum attainable static conductivity, showing that a larger fraction of the aqueous phase contributes to conductivity. There is no doubt that a corresponding shift would also be observed for the viscosity curves. Thus, a microemulsion behaves as an electrorheological fluid whose viscosity can be controlled by the electric field.

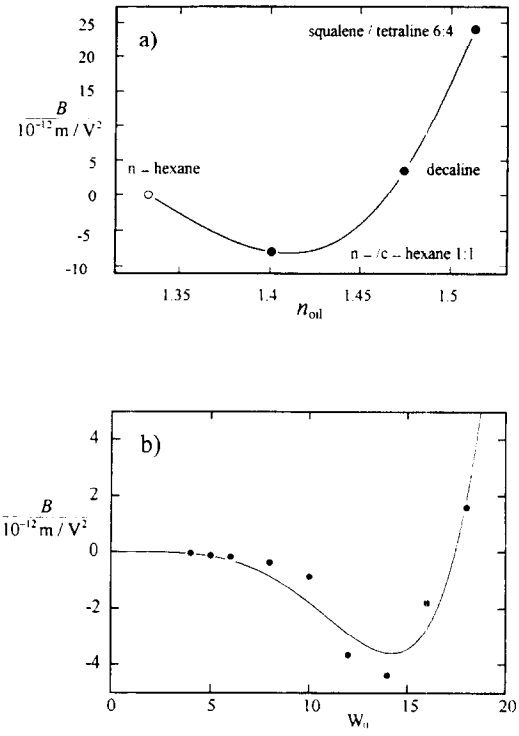

Fig. 6. Dependence of the Kerr-constant B on: (a) the refractive index of the oil in the system water/IG/oil ($W_0 = 24.5$, $c(\mathrm{IG})_{oil} = 0.186$ M) at a temperature $T = T_u - 1°C$, T_u denoting the upper phase boundary temperature. At these temperatures the systems consist of single droplets. In the system represented by an open circle ethyleneglycol was added to the aqueous phase in order to equalize the refractive indices of water and oil phase. (b) The droplet size (W_0 value) in the system water/decaline/IG ($c(\mathrm{IG})_{oil} = 0.186$ M) at $T = 25.0°C$. For droplets larger than about $W_0 \approx 17$, form birefringence exceeds the intrinsic birefringence of the surfactant molecules leading to a positive Kerr-effect. The solid line represents a fit with the polynomial given by Van der Linden et al. [32].

3.2.1. Amplitude of the Kerr-effect

There has been some discussion on the nature of the Kerr-effect. The finding of a positive birefringence in the AOT system led to the conclusion that form birefringence plays a significant role [30].

On the other hand, all our results so far with IG in different oils yielded a large negative value of the Kerr-constant, $B = \Delta n/\lambda \cdot E^2$, with a maximum up to $B \approx -5 \cdot 10^{-11}\mathrm{m/V^2}$ at the percolation point. Thus we concluded that form birefringence which is always positive for elongated particles oriented along the field does not play any significant role and the Kerr-effect is mainly due to the intrinsic anisotropy of the optical polarizability of the IG molecules ($\alpha_a > \alpha_b$). Generalizing this for all microemulsions, we suggested an inverse polarizability for the AOT molecule ($\alpha_a < \alpha_b$) [27]. However, under certain conditions we also find a positive Kerr-effect for the IG system (see Fig. 6) showing that this assumption is not justified.

This can be achieved by either changing the refractive index of the oil or the droplet radius. The dependence on the refractive index can be understood within the scope of the Peterlin-Stuart theory

for homogeneous ellipsoidal particles in a solvent [31], which proposes a nearly quadratic dependence of form birefringence as is found. The dependence on the droplet radius needs a more sophisticated theory, as has been worked out by Van der Linden et al. [32] who additionally consider the optical properties of the surfactant layer.

In order to obtain an estimation of the intrinsic birefringence of droplets deformed by an electric field one can adopt a simple approximation presented in the appendix. For a more rigorous treatment the reader is referred to [32].

3.3. Solute-induced percolation

Solute molecules dissolved in the aqueous or oil phase do generally shift the percolation curve and phase boundaries with respect to temperature. The shift of the phase boundaries with small molecules has been discussed in terms of the influence of the solute on the miscibility gaps of the binary water/surfactant and oil/surfactant systems [33]. In other cases, as for proteins, we certainly have to discuss more specifically the interaction of the solute with the surfactant membrane.

We have measured the shift of the percolation curve for various solutes, especially native and denatured proteins in order to learn about these interactions. Table 1 lists the concentration dependence of the percolation point for several solute molecules.

Table 1
Dependence of the percolation temperature on solute concentration for various solutes in AOT and IG systems

Solute (s)	$\partial T_p / \partial c(s)$ (°C·M^{-1})	
	AOT	IG
Potassium chloride	+494	–
Urea	−28.0	+3.0
Guanidinium chloride	+690	+11.0
Ethyleneglycol	−1.8	−2.8
Ethanol [a]	−9.2	–
Hexanol [a,b]	+340	
DIM [a]	+297	–
α-Chymotrypsin (nat.)	$+7 \cdot 10^4$	±0
Methemoglobin (den.)	-10^5	–

The concentration values are given with respect to the volume of water except [a] with respect to oil and [b] taken from [14].

3.3.1. Small molecules

In ionic AOT microemulsions a shift to lower temperature corresponds to a solute induced percolation, where the highly conducting water-continuous phase is already stabilized at lower temperatures. Effectively, there is an attractive interaction between droplets. This can be achieved with non-ionic polar molecules like urea, ethyleneglycol and other alcohols with a short aliphatic chain. A shift to higher temperatures, i.e., a stabilization of the droplet structure, is observed with long chain alcohols [14,34]. Table 1 shows that also DIM, with the same wedge shape as AOT, having a hydroxyl group instead of the ionic sulfonic group, behaves like other long chain alcohols. In terms of the microscopic picture, incorporation of wedge-shaped molecules forces the surfactant monolayer to adopt a more negative radius of curvature. There is a strong influence of salts, which also shift the percolation to higher temperatures. Here the influence of the electrostatics is dominant strengthening the counterion binding to the negatively charged AOT interfacial layer.

In the non-ionic IG microemulsions the effects of small molecules are reversed in temperature. Thus, solutes which induce percolation in the AOT system do so in the IG system as well, but the effect of lyotropic salts is only weak. Exceptions found so far are ethyleneglycol and guanidiniumchloride. The latter induces percolation and acts like urea (which is considered to be intercalated in the surfactant layer [35]) only in the IG system.

3.3.2. Proteins

The solubilization of enzymes in microemulsions has been investigated regarding the influence of the compartmentation on the enzyme and its activity [5,36] as well as with respect to the influence of the protein on the microemulsion properties [37,38].

It is known that native cytochrome *c* at neutral pH shifts the percolation curve to lower temperatures [6] while native chymotrypsin shifts it to higher ones [38]. In both cases the protein is positively charged. The isoelectric points are pH_i 10.6 for cytochrome *c*, and pH_i 8.1 for chymotrypsin.

We have found that methemoglobin induces percolation in AOT systems and is denatured as judged from the heme spectrum (see below). The percolation curves in Fig. 7a observed with increasing con-

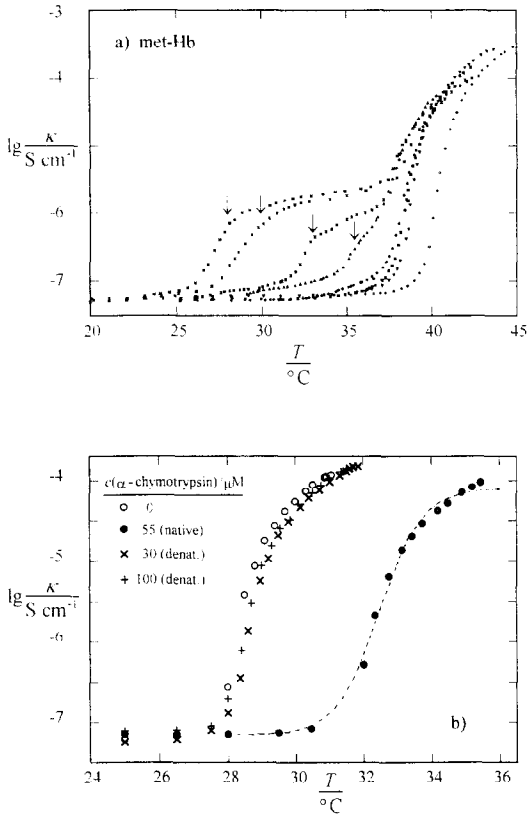

Fig. 7. Temperature dependence of the electric conductivity of AOT microemulsions (a) containing methemoglobin. With increasing concentration of methemoglobin the percolation curve is shifted to lower temperatures (solute induced percolation). The arrows mark the temperature threshold where methemoglobin starts to flocculate. System: AOT/n-heptane/aqueous methemoglobin. Curves from right to left: $c(\text{methb.})_{H_2O}$ = 0, 14.1, 32.6, 51.6, 60.7, 73.7, 82.9, 92.1 μM, respectively. $c(\text{methb.})_{\mu em} = c(\text{methb.})_{H_2O}/11$. (b) Containing α-chymotrypsin in native and denatured form (W_0 = 55.5, $c(\text{AOT})_{\text{n-heptane}}$ = 0.1 M, $c(\text{droplet})_{\mu em} \approx$ 40 μM, 0.01 M phosphate buffer, 0.5 M urea). Native α-chymotrypsin shifts the percolation temperature to higher values, whereas denatured protein shows no effect.

centration of methemoglobin show that the percolated systems are only stable up to a limiting protein concentration. Flocculation is observed when approaching the percolation point and the further conductivity increase corresponds to the low-concentration curve.

It seemed that denatured proteins, as well as native membrane proteins, interact with the surfactant layer and as a consequence induce percolation while native (non-membrane) proteins behave like salt does, although much more effectively.

To test this assumption, we have incorporated denatured α-chymotrypsin into the AOT-microemulsion. The protein was denatured in 5 M urea. This solution was then diluted 10-fold with water. The protein stays denatured under this condition as judged from the fluorescence at λ = 340 nm [39]. A microemulsion with this protein solution is compared with a microemulsion containing only 0.5 M urea in the aqueous phase. We have adopted this procedure, since a microemulsion of W_0 = 55.5 with very high urea concentration is not stable.

Fig. 7b shows that denatured α-chymotrypsin does not induce percolation, in fact there is no shift of the percolation curve at all. Furthermore, the shift of native chymotrypsin to higher percolation temperatures at pH 7 disappears at the isoelectric point, pH_i 8. It results that the influence of protein charge is more important, as has also been suggested by Pileni [6] from comparison of native with acetylated and succinylated cytochrome *c*. We conclude that the stabilizing effect of native chymotrypsin is due to the charges of the protein. The globular native protein at pH 7 with dimensions in the range of the droplet size has a positive net charge located at its surface. Interactions with the negatively charged surfactant layer are sufficient to reduce effectively the double layer charge density at the interface. In the denatured case there is no significant effect of the small concentration of charges in the micromolar range because due to the change in the secondary structure the charges are now distributed within the whole droplet.

In the IG system, where methemoglobin does not denature, methemoglobin and native as well as denatured chymotrypsin have no influence on the percolation curves. There is no apparent interaction with the membrane in these cases.

3.3.3. Hemin

The interaction of molecules with the AOT surfactant layer can directly be observed in the case of dissolved hemoglobin. As stated above, methemoglobin denatures and releases all its prosthetic protohemin groups. All four hemes are dissociated. Met-

hemoglobin in AOT microemulsions does not bind ligands like cyanide, azide, etc. any longer. Especially these low spin ligands have high binding constants in aqueous solution. It has been found in earlier measurements that the optical absorption spectra are dependent on the W_0 value of the microemulsion and thus on the size of the droplet [40]. This effect is due to the dimerization of the hemin. The induction of percolation and the W_0-dependence can also be observed when only hemin is solubilized in the microemulsion. We used deuterohemin, which lacks the vinyl groups, since we have better information on the dimerization equilibrium in water and ethyleneglycol–water mixtures for this molecule [10].

Fig. 8a shows the spectra of deuterohemin at different W_0 values. Increasing amounts of aqueous deuterohemin solution of constant concentration have been added to the oil/surfactant solution. The measured extinctions have been multiplied by the dilution factor in order to compensate for different total concentration.

The spectra are analogous to those of deuterohemin at various concentrations in aqueous solution. The appearance of an isosbestic point is a definite indication of the existence of an equilibrium between two forms, a monomeric form with a sharp band in the Soret region which is incorporated in the membrane and a dimeric form in the water core. In aqueous solution at pH 11 deuterohemin largely exists in its dimeric form with a dimerization equilibrium constant log $K_{\mathrm{dim}} \cong 7.4$, lowered to 5.3 in 25 vol.-% ethyleneglycol/water mixtures.

We analyzed the spectra in terms of the dimerization reaction (M denotes the monomeric and M_2 the dimeric form) $2M \rightleftarrows M_2$ with the apparent dimerization equilibrium constant $K_{\mathrm{app}} = c(M_2)/[c(M)]^2$ where all concentrations refer to the aqueous phase.

From the spectra in Fig. 8a the fraction of monomers α can be estimated, $\alpha = (E - E_\infty)/(E_0 - E_\infty)$. It is thereby assumed that the curve with $W_0^* = 18.5$ in 25 vol.-% ethyleneglycol represents the spectrum of the monomeric form (optical extinction E_0). The pure aqueous solution is taken for the dimeric form (E_∞). The apparent dimerization constant is calculated from $K_{\mathrm{app}} = (1 - \alpha)/2\alpha^2 c_0$ with $c_0 = 200\ \mu M$.

From Fig. 8b it is seen that a nearly linear relation results between the free energy of the dimerization and the water to surfactant ratio. An increase of K_{app} with the W_0 value (at constant surfactant concentration) is to be expected since there is more water available at larger W_0.

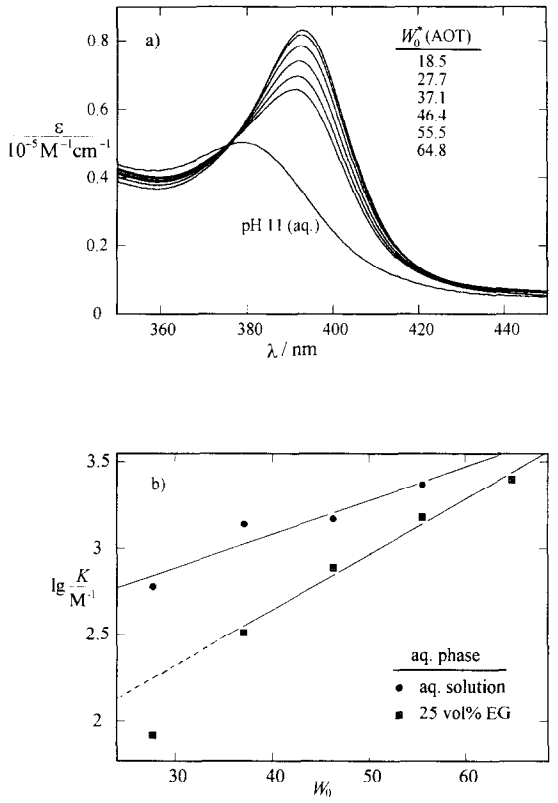

Fig. 8. Dimerization of deuterohemin in AOT/n-heptane microemulsions at different W_0 values: increasing volumes of a 200 μM deuterohemin solution in 3:1 v/v water/ethyleneglycol mixtures, pH 11 are added to the AOT/heptane solution. W_0^* is analogue to $W_0 = n_{H_2O}/n_{surf.} = V_{H_2O}/(\rho_{H_2O} M_{H_2O} n_{surf.})$ replacing V_{H_2O} by V_{H_2O+EG}. (a) Optical absorption spectra. The ordinate gives the apparent extinction coefficient with respect to the total volume. (b) Apparent dimerization constants in microemulsions with water and a v/v = 3:1 water/ethyleneglycol mixture at pH 11 as the polar phase containing a constant concentration of 200 μM deuterohemin.

The partition of hemin between the two phases can be understood by assuming a partition coefficient of the monomer independent of curvature of the surfactant layer. It remains to be established whether anomalies occur at still lower W_0 values, as has been observed in the analogous dimerization of acridine orange in AOT microemulsions [41].

3.3.4. Gelatin

Gelatin is another example of a denatured protein inducing percolation. AOT water in oil microemulsions with gelatin also reveal new aspects of molecular architecture. Haering and Luisi [42] have found that gels can be formed even in systems with a large volume fraction of the organic oil. These 'organogels' have been intensively studied by Quellet et al. [43] and Atkinson et al. [44]. We present some new electrooptic data giving information on the structure of these systems, restricting ourselves here to the non-gelled state.

Fig. 9a shows the temperature-induced conductivity percolation curves and Fig. 9b gives a detail of the phase diagram in the non-gelled region. The system shows no percolation in the gelatin-free state.

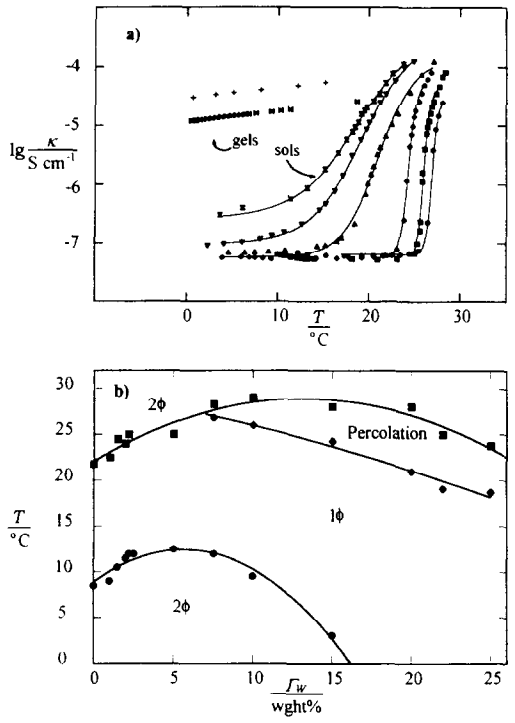

Fig. 9. Gelatin induced percolation in an ionic w/o-microemulsion system (0.1 M AOT in n-heptane, $W_0 = 61.7$). (a) T-induced conductivity percolation with increasing gelatin concentration (from right to left: $\Gamma_w = 7.5$, 10, 15, 20, 22, 25, 30, and 35 wt.-%, respectively). (b) Detail of the phase diagram with upper and lower phase boundaries and percolation line (constant composition of the microemulsion with respect to water, oil and amphiphile).

Phase separation occurs prior to percolation. Fig. 9a shows that increasing concentration of gelatin induces percolation. The gel state observed above a critical concentration of $\Gamma_w \approx 30$ wt.-% is characterized by a high conductivity throughout the accessible temperature range. There is a corresponding increase in the viscosities along the percolation transition. However, a strong increase with concentration is already found for the non-percolated state.

We will argue in the following that (i) the microemulsion droplets containing on the average but one gelatin molecule are not likely to keep their spherical shape but are distorted and may even have a configuration as that of gelatin in water, and that (ii) there occurs an internal transition at about half way before gelation begins.

These conclusions are derived from time resolved electric birefringence measurements.

Aqueous gelatin solutions already exhibit a Kerr-effect, obeying the Kerr-law at least up to 1 kV/cm; at 0.8 wt.-% gelatin we determined a Kerr-constant $B = 2 \cdot 10^{-11}$ m/V^2.

The field-on and field-off transient signals are not symmetric and the decay curve is not exponential (see Fig. 10), as is expected for random coil molecules [45]. Moreover the gelatin molecules have a broad molecular weight distribution.

Analysis in terms of stretched exponentials yields time constants around 0.1 ms and β values of about 0.5. Very similar values are obtained, if the average relaxation time, determined from the area under the decay curve is evaluated.

In Fig. 10 the transient signals of gelatin in water (a), the gelatin free microemulsion (b), and a gelatin-containing microemulsion (c) are compared. The concentration of $\Gamma_w = 2.2$ wt.-% corresponds to approximately one gelatin molecule per droplet. The gelatin-containing microemulsion shows a decay of the birefringence signal which is as slow as or even slower than that of the aqueous gelatin solution, whereas the microemulsion alone is considerably faster.

For a gelatin molecule within a spherical droplet a decay curve as fast as in the plain microemulsion is to be expected since there is no local electric field inside of the conducting droplet. As a consequence the slowing down of relaxation is due to a true orientation process as is the case in aqueous gelatin

solution. Thus one may envisage a gelatin molecule surrounded with a water layer coiling in the organic phase.

The decay relaxation time is constant in the lower concentration range (see Fig. 11), $\tau = 0.4$ ms ($\beta = 0.5$). From this value we can estimate an effective length of the orienting unit. According to the Zimm-model of the dynamics of a random coil in the non-draining case and the dilute regime, the longest relaxation time is determined by the radius of gyration and may approximately be calculated using the formula for the rotational diffusion coefficient of a sphere (for a detailed discussion see [45]).

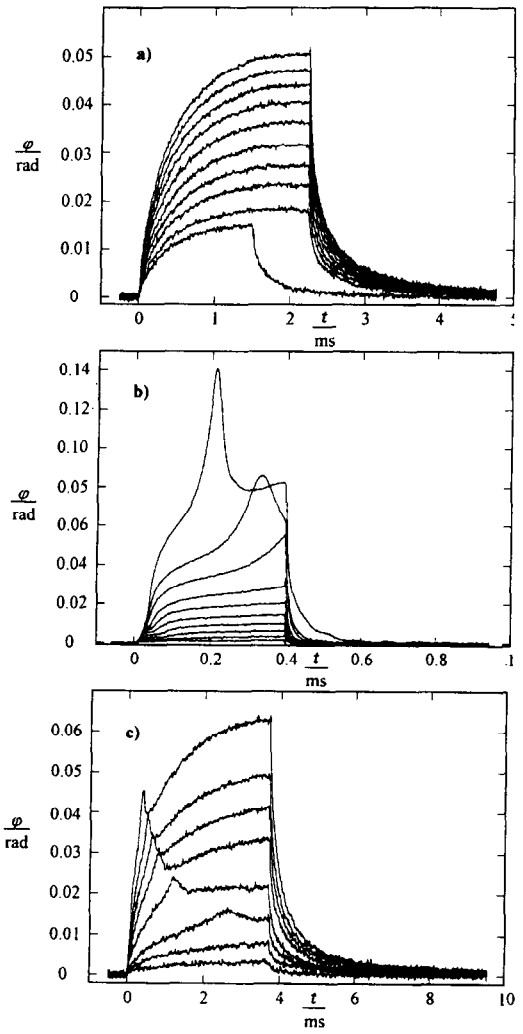

Fig. 10. Dynamic measurements of electro-optical birefringence with field strength as parameter. (a) aqueous gelatin gel ($\Gamma = 0.8$ wt.-%, $T = 12$°C) (b) gelatin-free microemulsion (0.1 M AOT in n-heptane, $W_0 = 61.7$, $\Gamma_w = 0$, $T = 16.8$°C). (c) gelatin containing microemulsion (0.1 M AOT in n-heptane, $W_0 = 61.7$, $\Gamma_w = 2.2$ wt.-%, $T = 17$°C).

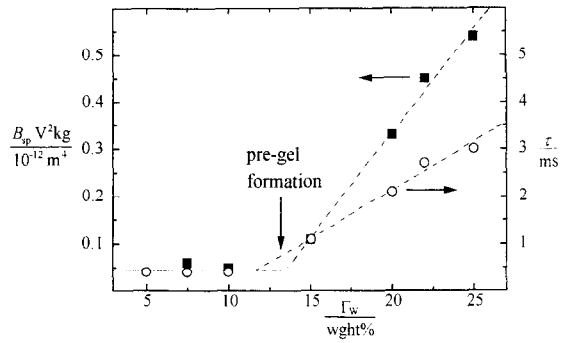

Fig. 11. Dependence of the specific Kerr-constants $B_{sp} = B/\Gamma_w$ and the relaxation times τ of the reorientation processes after the field pulse on the gelatin concentration. Both properties show a sudden increase at a gelatin concentration between 12 and 13 wt.-%. (0.1 M AOT in n-heptane, $W_0 = 61.7$. $\Delta T = T_p - T = 5$°C).

From $\tau = 1/6\theta_{rot} = 4\pi\eta R_g^3/3kT$ we obtain, using the viscosity of the oil, a radius of gyration $R_g = 190$ nm. This is quite a large value considering that the contour length is about 300 nm. Thus, several gelatin molecules seem to be linked together already at very low concentrations.

These gelatin aggregates may be in equilibrium with empty droplets as can be inferred from the birefringence signal in Fig. 10 where the gelatin containing microemulsion has a transient Kerr-signal which appears to be the sum of the signals of gelatin in pure water and the gelatin free microemulsion. The picture of a network structure in equilibrium with empty droplets has also arisen from the SANS investigations of Atkinson et al. [46].

Summarizing the observations on the system at low concentrations, one may state that under the given conditions the gelatin determines the structure of the microemulsion phase. We have evidence that this is not generally true and that there are conditions, at lower W_0 values, where the microemulsion droplets seem to remain intact up to a much higher concentration of gelatin.

It is seen from Fig. 11 that both the specific

Kerr-constant, $B_{sp} = B/\Gamma_u$, and the decay relaxation time are constant up to concentrations of about 12 to 13 wt.-% with respect to the aqueous phase (about 1.2 to 1.3 wt.-% with respect to the total volume), and then start to increase linearly with the gelatin concentration. This concentration thus clearly marks the transition from the diluted regime to a state where interactions between the solubilized gelatin chains begin. The drastic slowing down of the orientation process must be due to strong entanglement and possibly crosslinking between chains which may even form some 'pre-gel' state of the gelatin/microemulsion system.

Acknowledgements

We thank Kirsten Mönig for helping us with the measurements.

Appendix A. Estimation of the Kerr-effect of deformed droplets

This section gives a simple estimation of the intrinsic birefringence of droplets deformed by an electric field which already allows to understand the absolute value of the Kerr-constant. For a more rigorous treatment the reader is referred to [32]. We adopt the following approximation: the deformed drop is approximated by a cylinder with caps oriented in the direction of the field. The surfactant molecules stick perpendicularly to the surface with their long axis, i.e., the axis of the hydrocarbon chain. Only the molecules on the cylinder mantle contribute to the birefringence. If p denotes the ratio of diameter to length of the cylinder with caps, $p < 1$, the fraction of molecules contributing to the Kerr-effect is given by

$$\frac{N}{N_0} = 1 - p$$

where N_0 is the number density of surfactant molecules. These surfactant molecules lie in a plane perpendicular to the electric field with equal distribution of orientations, ϕ. Denoting α_a and α_b the optical polarizabilities along the long and short axis of the surfactant molecules, the difference of the refractive indices for light polarized parallel and perpendicular to the field is given by

$$\Delta n = n_{\parallel} - n_{\perp} = \frac{1}{2\epsilon_0} N(\alpha_{\parallel} - \alpha_b),$$

with $\alpha_{\parallel} = \alpha_b$, $\alpha_{\perp} = \alpha_b + (\alpha_a - \alpha_b)\sin^2\phi$.

Averaging over the orientations results in

$$\Delta n = -\frac{1}{4\epsilon_0} N_0(\alpha_a - \alpha_b)(1 - p)$$

If the optical polarizability along the long hydrocarbon chain axis is larger than along the radial one, the Kerr-effect is negative.

The electric field dependence of deformation of a droplet when only forces due to surface tension are considered, as has been derived by O'Konski and Thacher [47], and further extended by Mason and Allan [48], is given by

$$\frac{1-p}{1+p} = \frac{9\epsilon_0\epsilon}{16}\frac{R}{\gamma}E^2$$

where R = radius of the spherical droplet, γ = interfacial tension, ϵ = dielectric constant of the oil and E = electric field strength. Combining the above equations with the condition that p is close to 1, we arrive at:

$$B = \frac{9\epsilon_0}{32\lambda} N_0 \Delta\alpha \frac{R}{\gamma}$$

Introducing reasonable values for the polarizabilities ($\Delta\alpha/4\pi\epsilon_0 \approx 10^{-3}$ nm^3), the high value of the Kerr-constant can only be understood if the interfacial tension is as low as $\gamma \approx 10^{-5}$ Nm^{-1}. This is in accordance with the known behavior of microemulsion systems. If elastic properties of the monolayer dominate, γ has to be replaced by $K/2R^2$, where K denotes the bending rigidity [13,49].

The above equation for Δn can only be applied to the fast Kerr-process observed during the induction period of the electric current. The further increase in the Kerr-signal which parallels the current signal (see Fig. 4) is a manifestation of the additional orientation of surfactant interface when conducting water channels are formed in the process of droplet fusion.

References

[1] M. Kahlweit, in S.-H. Chen, J.S. Huang and P. Tartaglia (Eds.), Structure and Dynamics of Strongly Interacting Colloids and Supramolecular Aggregates in Solution, Kluwer, Dordrecht, 1992, p. 231.

[2] T.P. Hoar, J.H. Schulman, Nature, 152 (1943) 102.

[3] K. Shinoda and S. Friberg, Adv. Colloid Int. Sci., 4 (1975) 281.

[4] M. Kahlweit, R. Strey and G. Busse, J. Phys. Chem., 94 (1990) 3881.

[5] P.L. Luisi, Angew. Chem., 97 (1985) 449.

[6] M.P. Pileni, J. Phys. Chem., 97 (1993) 6961.

[7] S.-H. Chen, S.-L. Chang and R. Strey, J. Chem. Phys., 93 (1990) 1907.

[8] M. Kahlweit, R. Strey and R. Schomäcker, in W. Knoche and R. Schomäcker (Eds.), Reactions in Compartmentalized Liquids, Springer, Berlin, 1989, p. 1.

[9] L. Schlicht, Diplomarbeit, Universität zu Köln, 1992.

[10] Y. Gushimana, B. Doepner, E. Martinez-Hackert and G. Ilgenfritz, Biophys. Chem., 47 (1993) 153.

[11] F. Runge, W. Röhl and G. Ilgenfritz, Ber. Bunsenges. Phys. Chem., 95 (1991) 485.

[12] J.T. Overbeek, P.L. de Bruyn and F. Verhoeckx, in Th.F. Tadros (Ed.), Surfactants, Academic Press, London, 1984, p. 111.

[13] P. de Gennes and C. Taupin, J. Phys. Chem., 86 (1982) 2294.

[14] H.-F. Eicke, R. Kubick, R. Haase and I. Zschokke, in K. Mittal and B. Lindman (Eds.), Proc. Int. Symp., Surfactants in Solution, Vol. 3, Plenum, New York, 1984, p. 1533.

[15] F. Runge and G. Ilgenfritz, Physica A, 181 (1992) 69.

[16] D.J. Mitchell and B.W. Ninham, J. Chem. Soc., Faraday Trans. 2, 77 (1981) 601; J.N. Israelachvili, S. Marcelja and R.G. Horn, Quart. Revs. Biophys., 13 (1980) 121.

[17] J.D. Nicholson and J.H.R. Clarke, in K. Mittal and B. Lindman (Eds.), Proc. Int. Symp., Surfactants in Solution, Vol. 3, Plenum, New York, 1984, p. 1663.

[18] M. Laguës, J. Phys. Lett., 40 (1979) L331.

[19] A. Ponton, T. Bose and G. Delbos, J. Chem. Phys., 94 (1991) 6879.

[20] M.T. Clarkson, Phys. Rev. A, 37 (1988) 2079.

[21] S. Kirkpatrick, Phys. Rev. Lett., 27 (1971) 1722.

[22] B. Derrida, D. Stauffer, H.J. Herman and J. Vannimenus, J. Phys. Lett., 44 (1983) L701.

[23] D.B. Gingold and C.J. Lobb, Phys. Rev. B, 42 (1990) 8220.

[24] C. Cametti, P. Codastefano, P. Tartaglia, J. Rouch and S.-H. Chen, Phys. Rev. Lett., 64 (1990) 1461.

[25] A.T.J.M. Woutersen and C.G. de Kruif, J. Chem. Phys., 94 (1991) 5739.

[26] H.F. Eicke, R. Hilfiker and H. Thomas, Chem. Phys. Lett., 125 (1987) 106.

[27] F. Runge, L. Schlicht and J.-H. Spilgies, Ber. Bunsenges. Phys. Chem., 98 (1994) 506.

[28] E. Tekle, M. Ueda and Z. Schelly, J. Phys. Chem., 93 (1989) 5966.

[29] M. Ernst, in L. Pietronero and E. Tosatti (Eds.), Fractals in Physics, Elsevier, 1986, p. 289.

[30] H.F. Eicke and Z. Markovic, J. Colloid Int. Sci., 85, (1982) 198.

[31] A. Peterlin and H. Stuart, in Das Makromolekül in Lösung, Springer, Berlin, 1953, Chap. 7.

[32] E. van der Linden, S. Geiger and D. Bedeaux, Physica A, 156 (1989) 130.

[33] M. Kahlweit, R. Strey and D. Haase, J. Phys. Chem., 89 (1985) 163.

[34] M. Kahlweit, R. Strey and G. Busse, J. Phys. Chem., 95 (1991) 5344.

[35] F.C.L. de Almeida, H. Chaimovich and S. Schreier, Langmuir, 10 (1994) 1786.

[36] K. Martinek, A.V. Levashov, N. Klyachko, Y.L. Khmelnitski and I.V. Berezin, Eur. J. Biochem., 155 (1986) 453.

[37] J.P. Huruguen, M. Authier, J.L. Greffe and M.P. Pileni, Langmuir, 7 (1991) 243.

[38] P.D.I. Fletcher, G.D. Rees, B.H. Robinson and R.B. Freedman, Biochim. Biophys. Acta, 832 (1985) 204.

[39] T.P. Silverstein and L. Blomberg, J. Chem. Educ., 69 (1992) 852.

[40] D. Feustel, F. Runge and G. Ilgenfritz, in W. Knoche and R. Schomäcker (Eds.), Reactions in Compartmentalized Liquids, Springer, Berlin, 1989, p. 21.

[41] O. Ortona, V. Vitagliano and B.H. Robinson, J. Colloid Int. Sci., 125 (1988) 271.

[42] G. Haering and P.L. Luisi, J. Phys. Chem., 90 (1986) 5892.

[43] C. Quellet, H.F. Eicke and W. Sager, J. Phys. Chem., 95 (1991) 5642.

[44] P.J. Atkinson, B.H. Robinson, A.M. Howe and R.K. Heenan, J. Chem. Soc., Farad. Trans., 87 (1991) 3389.

[45] S. Wijmenga, F.v.d. Touw and M. Mandel, Macromolecules, 19 (1986) 1760.

[46] P.J. Atkinson, M.J. Grimson, R.K. Heenan, A.M. Howe and B.H. Robinson, J. Chem. Soc., Chem. Commun., (1989) 1807.

[47] Ch. O'Konski and H. Thacher, J. Phys. Chem., 57 (1953) 955.

[48] S. Mason and R. Allan, Proc. Roy. Soc. London A, 267 (1962) 45.

[49] B.P. Binks, J. Meunier and D. Langevin, Progr. Coll. Polym. Sci., 79 (1989) 208.